Viscoelastic behavior of polymeric foams: Experiments and modeling

Isadora R. Henriques, Lucie Rouleau, Daniel A. Castello, Lavinia A. Borges, Jean-François Deü

VISCOELASTIC BEHAVIOR OF POLYMERIC FOAMS: EXPERIMENTS AND MODELING

I.R. Henriques[1,2], L. Rouleau[1,*], D.A. Castello[2], L.A. Borges[2], J.-F. Deü[1]

[1]*Structural Mechanics and Coupled Systems Laboratory, Conservatoire National des Arts et Métiers (Cnam), Paris, France*
[2]*Mechanical Engineering Department, Universidade Federal do Rio de Janeiro (UFRJ), Rio de Janeiro, Brazil*

*Corresponding author.
Email address: lucie.rouleau@lecnam.net

Abstract

This work explores the viscoelastic behavior of two types of polymeric foams: an open-cell melamine foam and a closed-cell polyurethane foam. Experimental measurements were carried out on a torsional rheometer to estimate the complex shear modulus as a function of both temperature and frequency. A different and in some cases strong dependence of shear storage and loss moduli upon frequency and temperature was evidenced. The long-term viscoelastic behavior was then identified through the application of the time-temperature superposition principle. A fractional derivative model was properly calibrated to describe the behavior of each foam. This approach enabled two numerical simulations to further investigate the dissipation of mechanical energy. The first simulations explored hysteresis phenomena in cyclic loads in the time domain. The second tests analyzed their vibration damping performances in the low-frequency range. In both cases, only the viscoelasticity of the foam's skeleton was taken into account. The closed-cell polyurethane foam showed a greater ability to dissipate mechanical energy.

Keywords: Solid foams; Viscoelastic properties; Mechanical testing; Thermomechanical modeling; Damping

1. Introduction

Polymeric foams have been applied for different purposes and applications in recent years, ranging from packaging to aerospace industries (Gama *et al.*, 2018). The understanding of their frequency and temperature-dependent properties, as well as their mechanical behavior, are crucial for purposes of quality control and further improvements in product development and fabrication. They have thus become the focus of many experimental and numerical researches.

Generally speaking, polymeric foams are porous materials composed of a solid polymer skeleton (also called matrix) and air-filled pores. They can be separated into two main groups according to the nature of their polymer skeleton: thermoplastic and thermoset foams. Within these groups, they can even be differentiated according to their composition, cellular morphology, and other physical and thermal aspects. Their main features are resilience, lightweight, high porosity, good energy absorption, among others. All these features can be achieved or even improved by small modifications of their formulations (Khemani, 1997; Srivastava and Srivastava, 2014).

Due to their polymer skeleton, the mechanical response of such foams exhibits features of viscoelastic behavior. As a consequence, the mechanical properties of foams are time/frequency-dependent and viscoelastic phenomena such as relaxation, creep, hysteresis and load rate dependence can be observed. Temperature is another important factor that may also influence significantly their response (Ferry, 1980; Lakes, 2009).

To model the viscoelastic properties, fractional derivative models (Bagley and Torvik, 1983) has been employed. As for viscoelastic solids, these relations can describe reasonably well the behavior of foams with a limited number of parameters. Recently, Sahraoui and Zekri (2019) investigated the use of some fractional models to predict the frequency dependence of these properties over a broad range. The effects of some model parameters in the predictions were also highlighted.

From an experimental point of view, both quasi-static and dynamic techniques were developed over the years to assess their viscoelastic properties (Bonfiglio *et al.*, 2018; Jaouen *et al.*, 2008). Among these techniques, quasi-static torsion tests provide good estimations of the viscoelastic properties of the polymer skeleton as it ensures a constant volume during the test and a limited influence of fluid-structure interaction. This test consists in applying a sinusoidal excitation in torsion to a cylindrical sample and then measuring its response at different frequencies and temperatures, thus allowing the application of the well-known time-temperature superposition principle (TTSP) (Schwarzl and Staverman, 1952; Ferry, 1980) to overcome the limitations of the apparatus.

Furthermore, the dissipative properties due to viscoelasticity can be beneficial for certain applications. As pointed out by Rodriguez-Pérez *et al.* (2001), there is a great interest in studying the responses of polymeric foams to low-frequency vibrations as they have the potential to be used for passive damping of structures as constrained or extensional layers. Nonetheless, dissipation mechanisms vary according to material compositions and as a result, different performances may be observable (Ehrig *et al.*, 2018).

Bearing this in mind, this work has two main objectives. The first one is to experimentally measure the temperature and frequency-dependent viscoelastic properties of polymeric foams using dynamic mechanical analyzer (DMA) to properly calibrate numerical viscoelastic models. The second objective is to numerically investigate the dissipation of mechanical energy by these foams. The originality of this work is to relate, through finite element simulations, the viscoelastic properties of polymeric foams identified by DMA to their damping performance when used in dynamic applications. In this work, only the viscoelastic damping of the solid skeleton is considered as it is mainly responsible for the dissipation of mechanical energy in the low-frequency region. A fractional derivative model is used to describe viscoelastic behavior of foams. Two different foams are studied: an open-cell melamine foam and a closed-cell polyurethane foam. As evidenced in the first part of this paper, these materials have very different time-dependent behaviors which illustrates the wide variety of foams. Their damping performances are predicted, and results may provide guidelines for the practical use of polymeric foams as vibration mitigation materials.

This paper is structured as follows. In Section 2, the constitutive equations and the time-temperature superposition principle are presented. In Section 3, the experimental investigation is explained in detail. The tested materials, set-up and procedures are initially described. Then, the measurements are presented, the effects of frequency and temperature are highlighted, and a fractional model is calibrated. In Section 4, numerical simulations are performed to investigate the damping behavior of foams. Finally, the concluding remarks of this work are made in Section 5.

2. Modeling material's behavior

2.1. Linear Viscoelasticity

Different formulations to properly model the viscoelastic behavior based on mechanical analogs, internal variables, hereditary integrals and complex modulus concept can be found in the literature (Lakes, 2009). Under the assumptions of small strains and linear viscoelasticity, these constitutive equations are quite similar; each one having its own advantages and disadvantages. In particular, the use of fractional derivative operators may be attractive. Indeed, some advantages of this approach are the easy fitting of experimental measurements, the link between molecular theories and macroscopic behavior, the fulfillment of the second law of thermodynamics and the prediction of hysteresis loops (Dovstam, 2000; Enelung and Olsson, 1999). The general form of a one-dimensional constitutive equation based on this approach in the time domain is given by (Bagley and Torvik, 1983)

$$\sigma(t) + b_1 \frac{d^{\beta_1}}{dt^{\beta_1}}\sigma(t) + \ldots + b_n \frac{d^{\beta_n}}{dt^{\beta_n}}\sigma(t) = a_0\,\varepsilon(t) + a_1 \frac{d^{\alpha_1}}{dt^{\alpha_1}}\varepsilon(t) + \ldots + a_m \frac{d^{\alpha_m}}{dt^{\alpha_m}}\varepsilon(t) \quad (1)$$

where a_i and b_i are material constants, and β_i and α_i are the order of the fractional derivatives that must be within 0 and 1. The number of time derivatives m and n must satisfy the following thermodynamics restrictions: $m = n$ or $m = n + 1$.

In this work, the four-parameter fractional derivative model, also known as fractional Zener model, is adopted to describe the viscoelastic behavior of the analyzed foams. The mathematical and physical backgrounds of this particular fractional model were outlined by Pritz (1996). Thus, Eq. (1) reduces to

$$\sigma(\mathrm{t}) + \tau^{\alpha} \frac{d^{\alpha}\sigma(\mathrm{t})}{d\mathrm{t}^{\alpha}} = \mathrm{G}_0\, \varepsilon(\mathrm{t}) + \mathrm{G}_{\infty}\tau^{\alpha} \frac{d^{\alpha}\varepsilon(\mathrm{t})}{d\mathrm{t}^{\alpha}}, \tag{2}$$

where G_0 and G_∞ are, respectively, the relaxed and unrelaxed shear moduli, τ is the relaxation time and α is the order of the fractional derivative. Notice that these four parameters must obey the thermodynamic constraints (Bagley and Torvik, 1986) shown in Eq. (3) below to be physically meaningful.

$$G_\infty > G_0 \geq 0, \tau > 0 \text{ and } 0 < \alpha \leq 1 \tag{3}$$

As the experiments carried out in this work are in the frequency domain, it thus becomes interesting to express the constitutive equation described by Eq. (2) also in the frequency domain. Therefore, by the use of Fourier transform, the one-dimensional relationship between stress $\sigma^*(\omega)$ and strain $\varepsilon^*(\omega)$ is expressed as

$$\sigma^*(\omega) = \left[G_0 + (G_\infty - G_0)\frac{(j\omega\tau)^{\alpha}}{1 + (j\omega\tau)^{\alpha}}\right]\varepsilon^*(\omega) = G^*(\omega)\varepsilon^*(\omega), \tag{4}$$

where $j = \sqrt{-1}$ is the imaginary number, ω is the angular frequency in radians per second and $q^*(\omega)$ denotes the Fourier transform of a variable $q(t)$. As for $G^*(\omega)$, it corresponds to the complex shear modulus that can be divided into its real and imaginary parts, respectively, known as shear storage $G'(\omega)$ and loss $G''(\omega)$ moduli. The ratio between these two components $\eta(\omega) = G''(\omega) / G'(\omega)$ is known as loss factor and can be used as a key indicator of damping performance.

Moreover, under the assumption of constant Poisson ratio, all the mechanical moduli have the same frequency dependence, so the one-dimensional constitutive law can be extended in three dimensions (Makris, 1997):

$$\sigma_{ij}^*(\omega) = 2G^*(\omega)\left(\varepsilon_{ij}{}^*(\omega) + \frac{\nu}{1-2\nu}\varepsilon_{kk}{}^*(\omega)\delta_{ij}\right), \tag{5}$$

where δ_{ij} is the Kronecker delta.

2.2. Time-temperature Superposition Principle (TTSP)

The time-temperature superposition principle (TTSP) is an empirical principle that gives an equivalence between the mechanical properties measured at a temperature T and a frequency ω and those measured at a reference temperature T_0 and a reduced frequency ω_R. It consists in applying horizontal and vertical shifts to isotherms just above or below T_0 to superimpose them in a single master curve to study the long-term behavior (Schwarzl and Staverman, 1952; Ferry, 1980).

From the mathematical point of view, this principle is expressed as

$$b_T(T,T_0)G^*(\omega,T) = G^*(\omega_R,T_0), \tag{6}$$

where $\omega_R = a_T(T,T_0)\omega$ is the reduced frequency, and $a_T(T,T_0)$ and $b_T(T,T_0)$ are, respectively, the horizontal and vertical shift factors which depend on the material and on the reference temperature T_0 chosen for the analysis.

In this work, the horizontal shift factor $a_T(T,T_0)$, also known as thermal shift factor, is modeled by the Williams-Landel-Ferry equation (WLF) (Williams *et al.*, 1955) as follows

$$\log a_T\ (T,T_0) = -\frac{C_1\,(T-T_0)}{C_2 + (T-T_0)}, \tag{7}$$

where T is the temperature in Kelvin and C_1 and C_2 are empirical constants that depend on the material and the reference temperature T_0, which have an order of magnitude of 10 and 100K, respectively (Ferry, 1980). This is an empirical relationship based on the assumption that the fractional free volume of polymers increases with temperature above its glass transition temperature.

As for the vertical shift factor $b_T(T,T_0)$, the Bueche-Rouse theory is herein adopted (Dealy and Plazek, 2009). It assumes that the material property is proportional to the product of the mass density ρ and the temperature T such that

$$b_T(T,T_0) = \frac{T_0\rho_0}{T\rho}, \tag{8}$$

where ρ_0 is the mass density at the reference temperature T_0.

An important point that should be highlighted is that this principle is only applied to the viscoelastic materials said to be thermo-rheological simple (Schwarzl and Staverman, 1952; Ferry, 1980). In other cases, this hypothesis cannot be expected to work (Lakes, 2009). Therefore, the validity of this assumption and the applicability of the TTSP must be verified for the analyzed material. The Cole-Cole diagram (Dae Han and Kim, 1993) and the Black space or Wicket plot (Gurp and Palmen, 1998) are two simple ways to check it. Furthermore, these diagrams also indicate the need for vertical shifting (Rouleau *et al.*, 2013).

3. Experimental Set-up

3.1. Materials and Samples Preparation

Two different polymeric foams are investigated: an open-cell melamine foam (hereinafter referred to as foam A) and a closed-cell polyurethane foam (hereinafter referred to as foam B). The foams under study were industrially produced and the manufacturing processes are not known. Nevertheless, they were part of the five porous materials characterized in an interlaboratory campaign on the dynamic elastic properties of poroelastic media. The measurement results presented in Bonfiglio *et al.* (2018) have shown that these two particular foams can be considered as homogeneous and almost isotropic. Therefore, these two hypotheses are considered in this work.

Cylindrical samples, having a diameter of 24 mm and a wall thickness of 25 mm, were cut off from the same block of material as shown in Fig. 1. According to ISO 6721-7 (2019), the dimensions are not critical as length corrections are applied to account for clamping effects. This limited a possible issue of heterogeneity between samples and so, spatial homogeneity was assumed hereinafter. As an attempt to control sample size and limit possible edge effects, gasket punches were used to perform the cut.

Table 1 presents the nomenclature adopted, selected properties and samples dimensions, whereby the foams are sorted by density. Cell type, Poisson's ratio ν, density ρ and airflow

resistivity σ_r were given by Bonfiglio *et al.* (2018). The glass transition temperature T_g was determined by a standard differential scanning calorimetry (DSC) following ISO 11357-2 (2013). It should be highlighted that the value of Poisson's ratio is a representative one chosen from the experimental results presented in Bonfiglio *et al.* (2018). Despite the observed variability of Poisson's ratio with the characterization procedure, it has been shown that both foams have almost constant Poisson's ratio over a wide frequency range. Therefore, it is herein assumed to be real-valued and frequency independent. This feature of foams has been evidenced in previous experimental works such as Mariez *et al.* (1996), Etchessahar *et al.* (2005) and Jaouen *et al*. (2008). Thereby, all foam's mechanical moduli have the same frequency dependence.

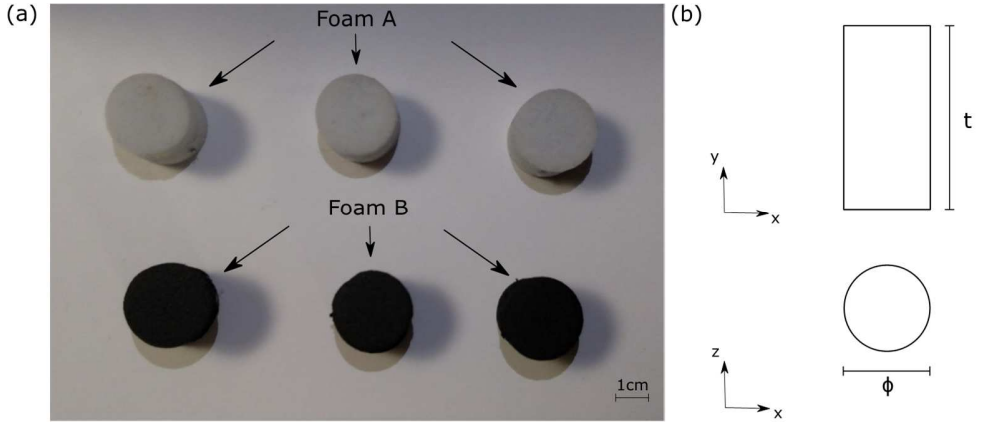

Fig. 1. Samples used for tests. (a) Photograph and (b) scheme.

Table 1 Description of the tested materials, where $\boldsymbol{t}$ is the nominal thickness, $\boldsymbol{\phi}$ is the nominal diameter, $\boldsymbol{\nu}$ is the Poisson's ratio, $\boldsymbol{\rho}$ is the nominal density, $\boldsymbol{\sigma_r}$ is the airflow resistivity and $\boldsymbol{T_g}$ is the glass transition temperature.

Foam	Material Base	Cell Type	t [mm]	ϕ [mm]	ν	ρ [kg/m^3]	σ_r [Pa.s / m^2]	T_g [°C]
A	melamine	open	25	24	0.3	10	10000	n/a
B	polyurethane	closed	25	24	0.35	48	-	-35.5

3.2. Test conditions

Dynamic tests were carried out using a commercial torsional rheometer (Anton Paar MCR 502), as shown in Fig. 2(a), to measure the complex shear modulus $G^*(\omega)$. The schematic diagram of this experimental set-up is illustrated next in Fig. 2(b). A detailed description of this method can be found in the work of Etchessahar *et al.* (2005).

The measurements were performed in torsion mode varying both temperature and frequency. Frequency sweeps from 0.1 to 20Hz, representing a total of 13 different frequencies, were carried out at four temperatures from -10 to 20°C. The dynamic strain was set to 0.1% to remain in the linear viscoelastic regime. This value was verified by a previous strain sweep test at 20°C, with a constant frequency of 1Hz.

At least three samples of each material were tested to reduce the risks of abnormalities due to the fabrication process or experimental errors. The normal statistics of sampling was performed to determine the repeatability of these tests. Besides, mechanical calibrations were carried out before each set of tests of each material.

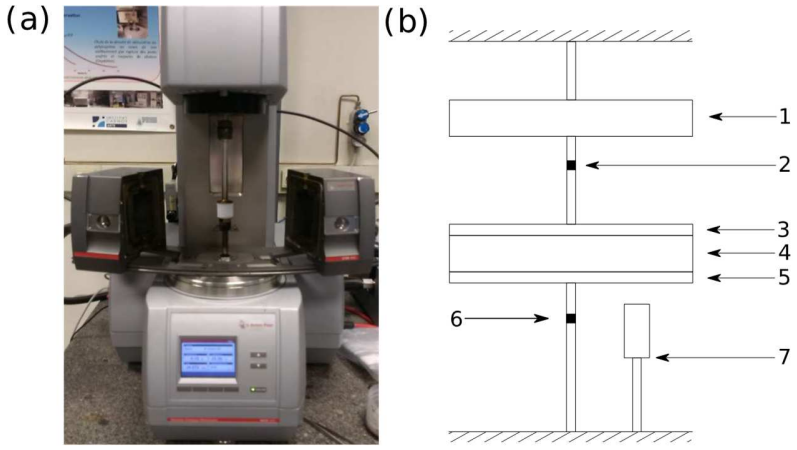

Fig. 2. Experimental set-up. (a) Rheometer MCR 502 from Anton Paar. (b) Schematic diagram of the rheometer main components; (1) torsional motor, (2) torque transducer, (3) rotationary plate, (4) foam sample, (5) supporting plate, (6) angular displacement transducer and (7) thermometer.

3.3. Results and Discussion

The temperature and frequency-dependent viscoelastic properties of two different types of foams were experimentally determined, as previously described in subsection 3.2. Figures 3 and 4 show the measurement results for the shear storage and loss moduli, respectively denoted by $G'(\omega)$ and $G''(\omega)$, as a function of the applied frequency at different temperatures. They are presented as the mean of the samples measured together with the corresponding standard deviation. When carefully analyzing this set of raw data, one may conclude that higher temperatures lead to higher standard deviations, especially for the loss modulus of foam A shown in Fig. 3(b). But despite that, the tests had a good reproducibility as the standard deviations presented low amplitudes on the full analyzed range. Furthermore, it can be seen that the effects of temperature and frequency were not the same for these materials.

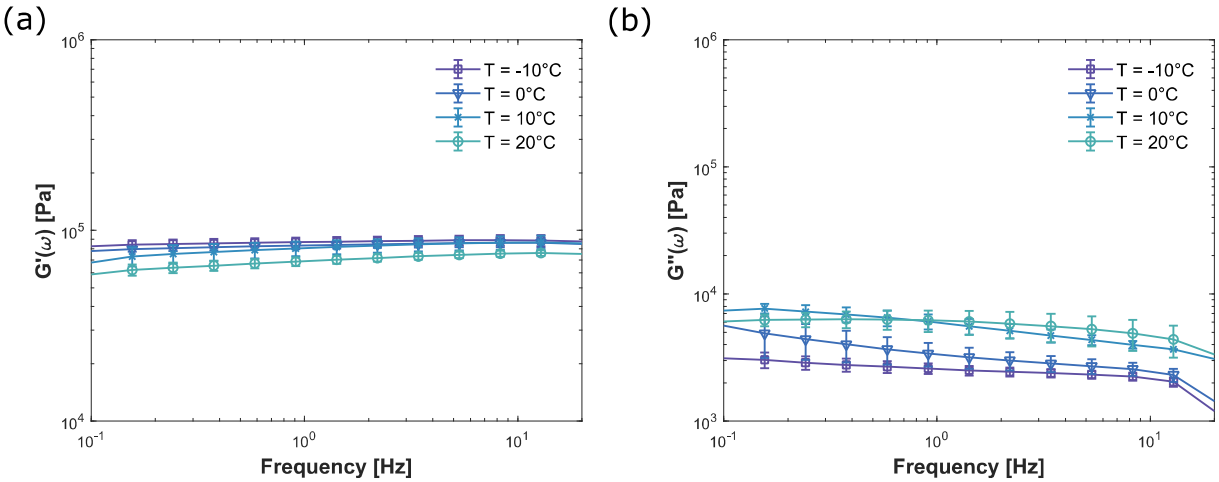

Fig. 3. DMA measurements for foam A. (a) Storage and (b) loss moduli.

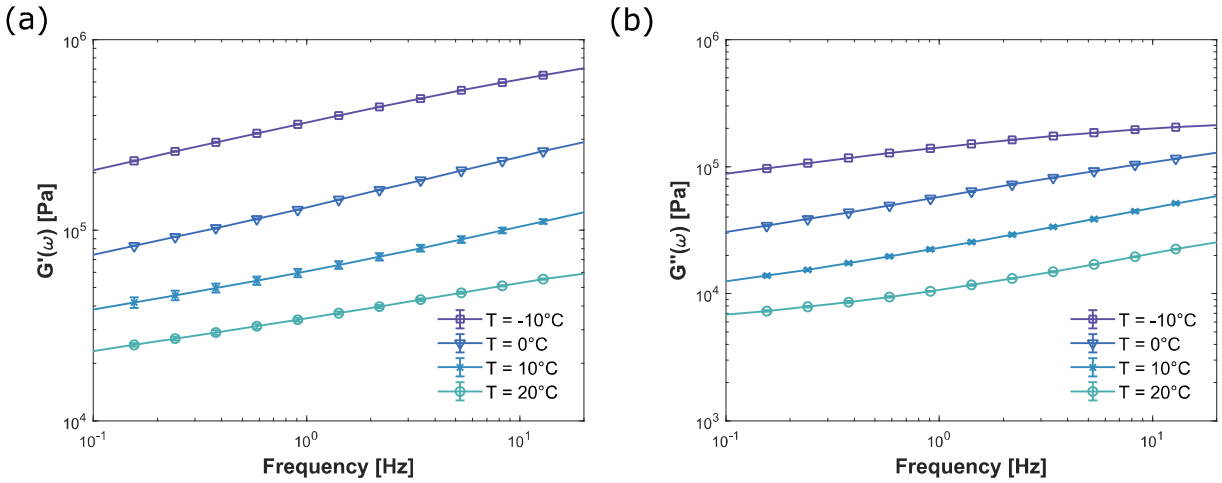

Fig. 4. DMA measurements for foam B. (a) Storage and (b) loss moduli.

From Fig. 3, one can note that the storage modulus increased with frequency and decreased with temperature, whereas the loss modulus had opposite behavior. Nevertheless, increasing temperature and/or frequency did not lead to great changes in moduli values for foam A. The values and the variations of storage and loss moduli with temperature and frequency are very similar to those obtained for the same foam by other characterization procedures (Bonfiglio *et al.*, 2018) and to those measured in (Jaouen *et al.*, 2008) on another melamine foam. In some other studies (Cuenca *et al.*, 2014; Sahraoui *et al.*, 2015), the loss modulus is found to be increasing with frequency and decreasing with temperature. However, the dependence of moduli on both parameters is also weak and their values are still consistent with the measurements presented in Fig. 3.

From Fig. 4, one can observe that foam B shows, on the other hand, strong viscoelastic dependence. Both shear storage and loss moduli decreased significantly with temperature: by about a decade. However, they increased with the loading frequency; for this test condition, the sensitivity to frequency variations decreased as temperature increased. As for foam A, similar values of moduli and parameters dependency can be observed in the results from other experimental methods for foam B (Bonfiglio *et al.*, 2018). Moreover, these results are consistent with other previous works (Etchessahar *et al.*, 2005; Sfaoui, 1995) on other polyurethane foams.

Comparing the results obtained for these two different foams, the differences observed in the patterns of the curves are inherent to their viscoelastic behavior. Measurements were performed before the glass transition of foam A and after the glass transition of foam B (see Table 1 for T_g values). Therefore, both foams were tested in different regions of viscoelastic behavior. Moreover, considering the investigated range of frequency and temperature, foam B has a greater capability of storing and dissipating energy than foam A. It thus can be inferred that these foams have different time-dependent behavior.

Afterward, the hypothesis of thermo-rheological simple behavior and the applicability of the TTSP for both foams were checked by plotting Cole-Cole and Black diagrams, as shown in Figs. 5 and 6 below. When considering the variance of experimental data, most points lied close to one continuous curve in both diagrams. The differences observed in both diagrams between foam A and foam B strengthens the idea that they were tested in distinct regions of viscoelastic behavior: in the glass transition region for foam B and in the glassy plateau for foam A. Some points from the measurements of foam A, however, deviated from the curves at high frequencies and they

may be related to experimental difficulties concerning DMA measurements such as resonance phenomena (Placet and Foltête, 2010) and preload (Bonfiglio *et al.*, 2018; Butaud *et al.*, 2018). In this regard, these points were not considered for the generation of the master curves of this foam (Fowler and Rogers, 2006; Rouleau *et al.*, 2015).

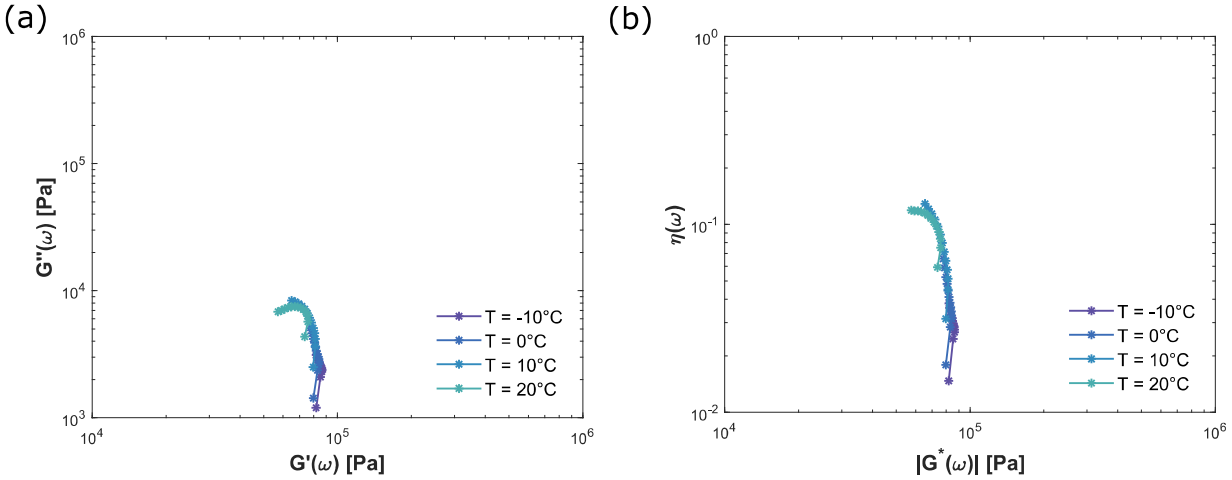

Fig. 5. Validation of thermo-rheological simple behavior of foam A. (a) Cole-Cole and (b) Black diagrams.

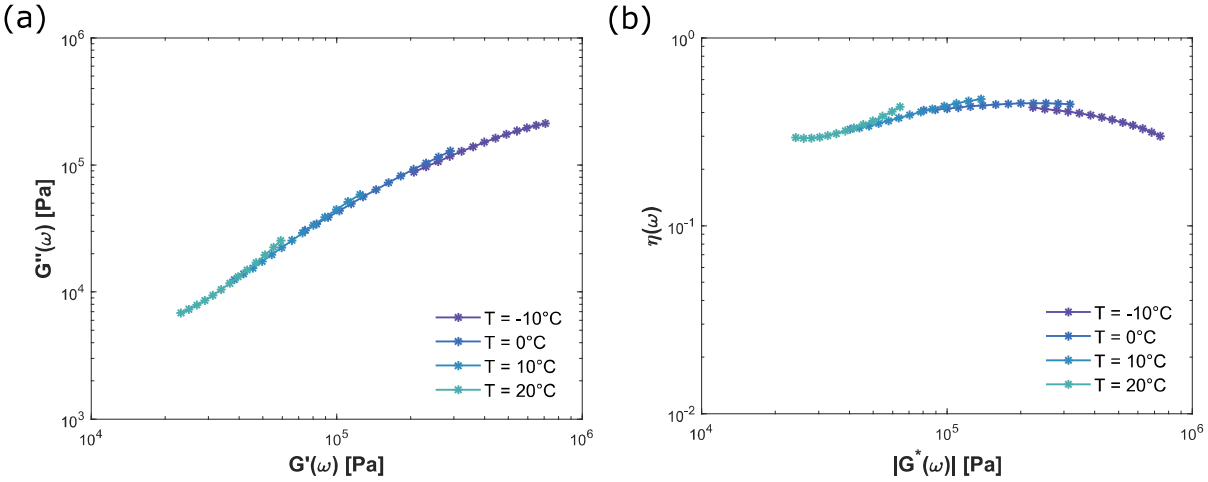

Fig. 6. Validation of thermo-rheological simple behavior of foam B. (a) Cole-Cole and (b) Black diagrams.

The horizontal shift factors needed for the application of the TTSP were estimated at the reference temperature T_0 = 20°C using the method proposed by Rouleau *et al.* (2013), which ensures the fulfillment of the Kramers-Kronig relations conveying the causality condition. Since the dependence of the storage and the loss moduli of foam A with temperature is weak, it is important not to rely on shifting techniques merely based on the least square method to generate master curves. Hence, the horizontal shift factors were fitted by the WLF equation to verify the coherence of their values, as illustrated in Fig. 7. The empirical constants C_1 and C_2 leading to a good fit with the optimized shift coefficients were, respectively, 9.80 and 115.08K for foam A, and 17.99 and 153.03K for foam B. The vertical shift coefficients b_T were found equal to 1 for both foams, which is consistent with constant linear thermal expansion coefficients on the temperature range investigated. Therefore, the measured isotherms were horizontally shifted

according to the corresponding shift factor $a_T(T, T_0)$, except the one related to the reference temperature.

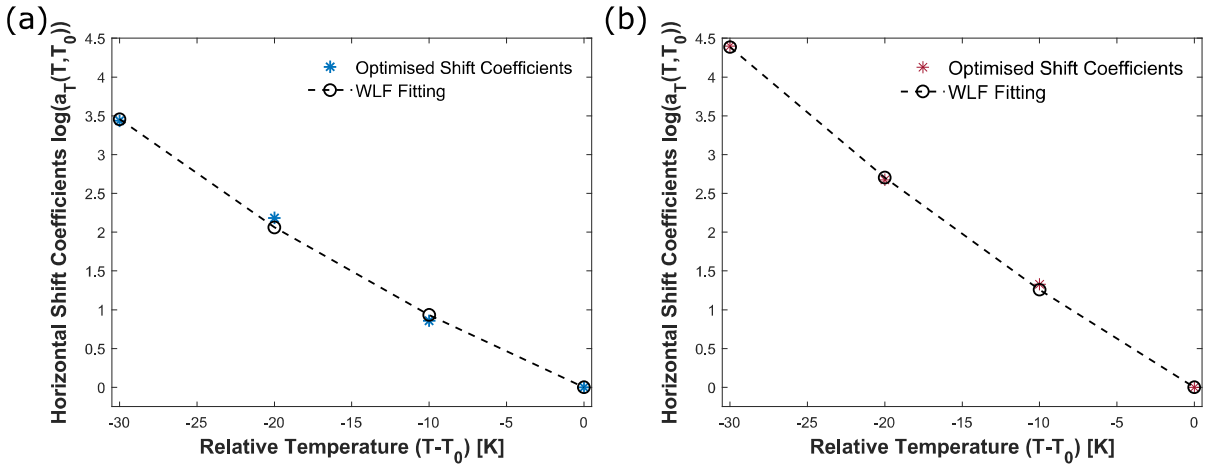

Fig. 7. Horizontal shift coefficients for (a) foam A and (b) foam B. The optimized coefficients are fitted by WLF equation.

The experimental master curves were built at 20°C, exhibiting thus the moduli behavior over a large frequency range up to approximately 10^6 Hz. A four-parameter fractional derivative model was then calibrated to describe the frequency-dependency of the complex shear modulus, as explained in subsection 2.1. Table 2 gives the four viscoelastic parameters G_0, G_∞, τ and α estimated by the least square method for both foams. One can notice that the thermodynamic requirements expressed in Eq. (3) were satisfied.

Table 2 Estimated fractional derivative model parameters

Foam	G_0 [Pa]	G_∞ [Pa]	τ [s]	α
A	4.79×10^4	8.63×10^4	1.32×10^{-1}	0.43
B	1.31×10^4	2.11×10^6	4.70×10^{-7}	0.30

Figures 8 and 9 show the experimental master curves together with the calibrated model. The relaxation phenomenon, closely related to the increase of complex modulus with frequency, can be observed. This feature is a consequence of molecular rearrangements in the polymer chains, which can be even permanent causing deformation in the material, to reduce internal energy. In (Jaouen *et al.*, 2008), a relaxation time of 0.084 s was found for a melamine foam, which is close to the relaxation time identified for foam A. However, it should be noted that very different values of relaxation time were reported in the literature for melamine foam: from 10^{-5} s in (Cuenca *et al.*, 2014) to 2 x 10^{-7} s in (Geslain *et al.*, 2011). For foam B, a relaxation time of 10^{-5} s was reported in (Sahraoui and Zekri, 2019).

Comparing the experimental and model curves, it is possible to observe that, for foam A, the model adopted can properly describe the shear storage modulus, but it has some difficulties in describing the shear loss modulus, especially at higher frequencies. This difficulty may be related to the lack of experimental data at higher temperatures. This aspect is a limitation of the experimental set-up: the sample was glued using a double-sided adhesive tape whose properties would have probably affected the measurements at higher temperature. For foam B, on the other hand, experimental and model curves presented high levels of correlations for both shear storage and loss moduli.

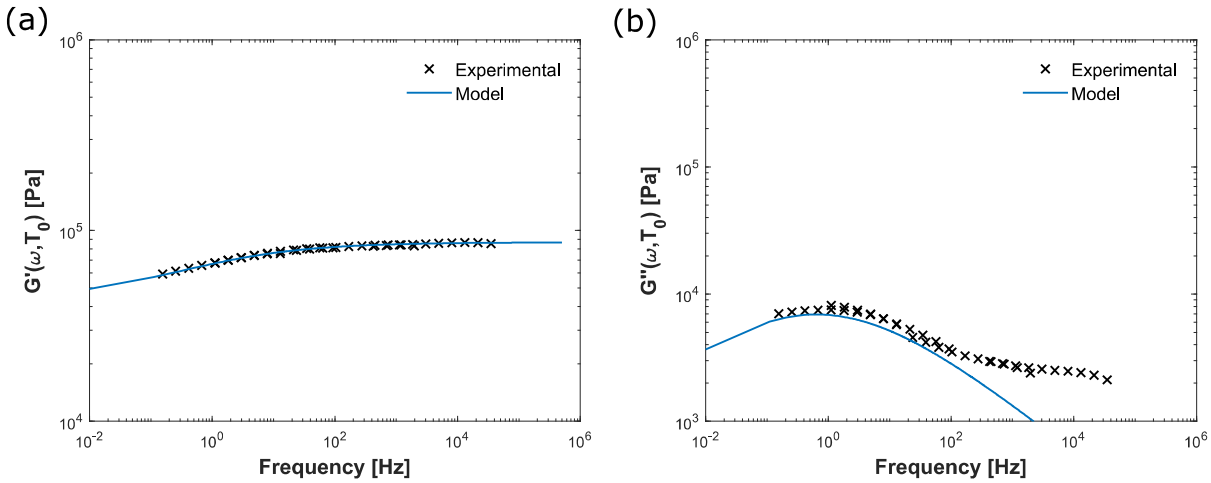

Fig. 8. Master curves for foam A at T_0 = 20°C. (a) Storage and (b) loss moduli.

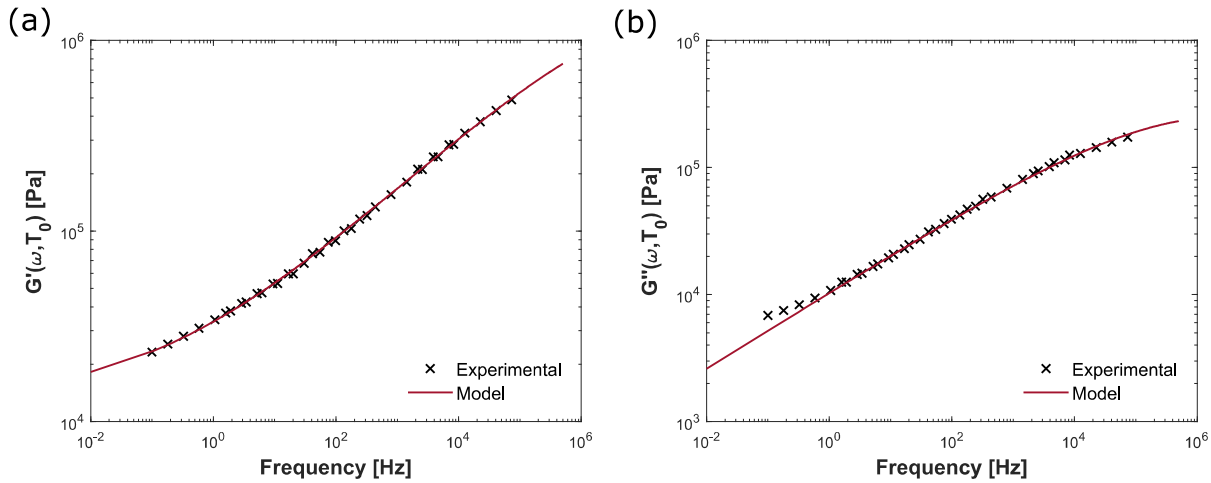

Fig. 9. Master curves for foam B at T_0 = 20°C. (a) Storage and (b) loss moduli.

The calibrated viscoelastic models of the investigated foams are further compared in Fig. 10, where the moduli amplitudes, $|G^*(\omega)|$, and loss factor, $\eta(\omega)$, are both depicted as a function of frequency. As highlighted by a black solid line in Fig. 10(a), two different regions of behavior are observed. Initially, at low frequencies, the moduli amplitude of foam A was higher than the one of foam B. But the difference between these amplitudes reduced as frequency increased, becoming zero at about 41-42 Hz (highlighted in the graph by a black circle). From this point on, foam B had a higher modulus and the difference between the values increased with frequency. From the curves of loss factor shown in Fig. 10(b), it is possible to infer that foam B presents a higher damping capability than foam A on the whole frequency range. Indeed, foam A showed very light damping: loss factor was within the range [10^{-3}, 10^{-1}] with a maximum value of,

approximately 0.12 at about 0.25 Hz. Foam B, in turn, evidenced moderate damping: loss factor varied between 10^{-1} and 10^{0} with a maximum of 0.48 at 320Hz. It is worth mentioning that these estimates were obtained for the reference temperature T_0 = 20°C and they change with temperature. Nevertheless, with the models calibrated, one can predict them at any desired temperature by means of the TTSP.

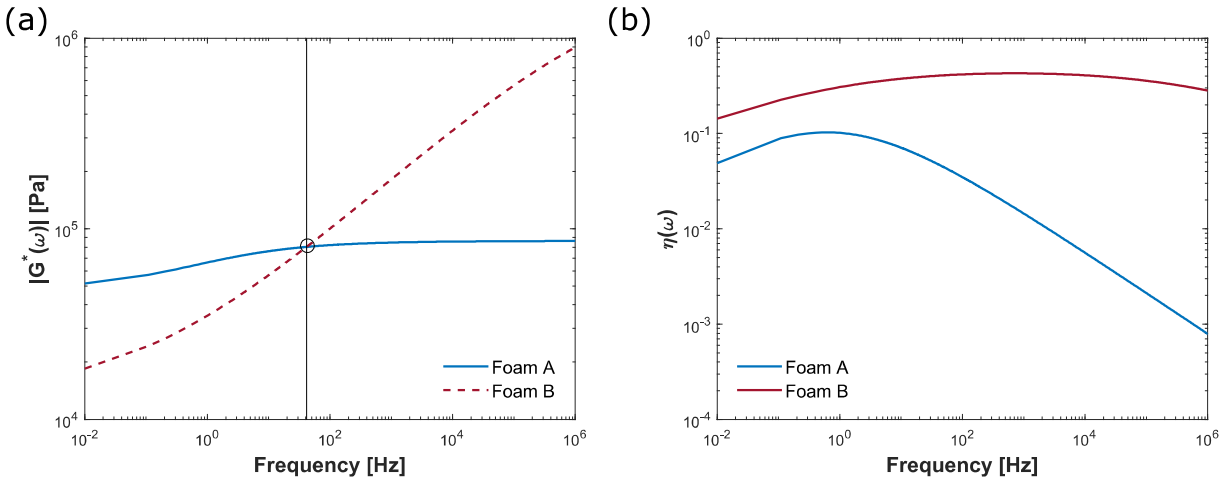

Fig. 10. Comparison between the calibrated models of foam A and foam B at T_0 = 20°C. (a) Moduli amplitude and (b) loss factor.

Some aspects should be highlighted here concerning the master curves show in Figs. 8 to 10 inasmuch as caution must be taken when considering the mechanical properties extrapolated at high frequencies. The first point is that measurements were performed in torsion within a low-frequency range where the coupling between the solid and the fluid phase is weak. At higher frequencies, this coupling may influence the dynamic characteristics of foams even though classical dynamic mechanical analyses do not take this coupling into account. Nevertheless, despite these facts, one may emphasize that the dynamic properties up to 10^4 Hz are consistent with the properties measured by other characterization techniques of the same materials (Bonfiglio et al., 2018). Similar values were also reported for this class of materials in the literature (Cuenca *et al.*, 2014; Etchessahar *et al.*, 2005; Jaouen *et al.*, 2008; Sahraoui *et al.*, 2015).

4. Numerical Simulations

Once a viscoelastic model is properly calibrated to describe the material's behavior, a range of analyses can be performed. This section presents two numerical investigations focusing on the mechanical energy dissipated by these foams using the calibrated four-parameter fractional derivative model at 20°C. The first investigation is concerned with the energy dissipation due to a loading-unloading cycle in the time domain. The second one, in turn, is dedicated to the evaluation of the vibration damping performance of these foams when bonded on an elastic structure in the frequency domain.

The goal here is to relate material properties with the damping performance of foams in low-frequency dynamic applications. In this way, it could help designing damping solutions based on foams. For instance, the time-domain response of foams to loading-unloading cycles is of interest when studying shock and vibration isolation during shipping and transportation in packaging applications. In the second numerical study considered in this section, the goal is to investigate the potential use of foam layers as passive damping of structures in the low-frequency

domain. There is an interest in the automotive industry to replace heavy rubber layer with dissipative foams.

It should be highlighted that both analyses neglect the air-skeleton interactions since they are performed in the low frequency range. From a physical point of view, in closed-cell foams, the pressure caused by the presence of air in the pores contributes to the material's stiffness. In open-cell foams, on the other hand, the air can escape when the material is under loading conditions. However, the air flow does not have a great influence when the material is subjected to quasi-static conditions or excited in the low-frequency range (Lakes, 2009). Thereby, the investigated polymeric foams are considered as monophasic viscoelastic solids and the frequency dependence of viscoelastic properties is taken into account. Furthermore, in the work of Dauchez *et al.* (2003), this intrinsic mechanical dissipation related to the viscoelastic solid skeleton has been pointed out to play a major role in the analyzed low-frequency range.

4.1. Cyclic Loading Test

As explained in Section 2, one of the phenomena observed in viscoelastic materials is a hysteresis in a stress-strain curve when a cyclic loading is applied. The amount of dissipated energy during a loading-unloading cycle is expressed by the area within the hysteresis loop, which may vary according to loading rate and temperature (Ferry, 1980; Lakes, 2009).

In this first study, we are interested in the energy dissipated in a viscoelastic polymeric foam when subjected to loading cycles. One-dimensional transient analyses are realized for two prescribed stress histories as shown in Fig. 11. For both situations, three linear loading-unloading cycles were applied to the material. They are performed such that the maximum prescribed stress levels are successively increased: 1.0 Pa, 2.0 Pa and 3.0 Pa. The difference between them relies on the very distinct time scales, about 10^0s in the first case and 10^{-3} s in the second one.

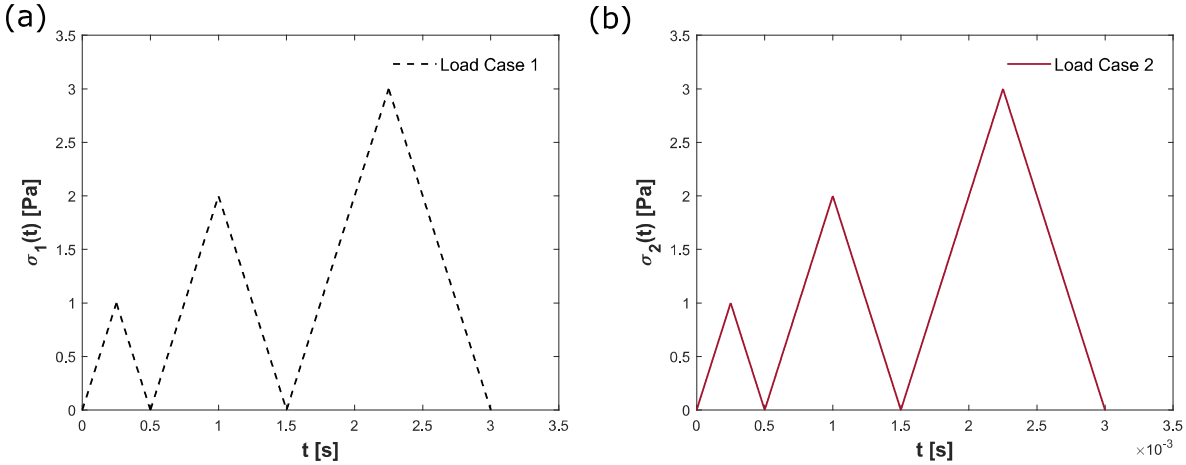

Fig. 11. Prescribed stress histories for cyclic tests. (a) Load case 1 and (b) load case 2.

Since Eq. (2) does not have any analytical solution, the numerical approach based on triangular strip matrices proposed by Podlubny (2000) is implemented. This approach consists in solving a linear ordinary fractional differential equation by formulating a system of algebraic equations, rather than using recurrence relations. The reader is referred to Podlubny (2000) for further details.

Figure 13 shows the stress-strain curves obtained for the two loading-unloading cases, considering a reference temperature of 20°C. It is possible to observe hysteresis loops in all scenarios. This is even more evident for foam B, highlighting its viscoelastic behavior and its potential capability to be used in damping systems. Furthermore, for both foams, the dissipation of mechanical energy is dependent upon the stress applied and its rate. The higher the maximum

stress level, the greater the percentage of dissipation per cycle. Additionally, they all exhibit a lower energy loss in the second load case whose stress rate was 10^3 times higher than the first case. This means that aspects of elastic behavior are more predominant than the viscous ones, especially for foam A.

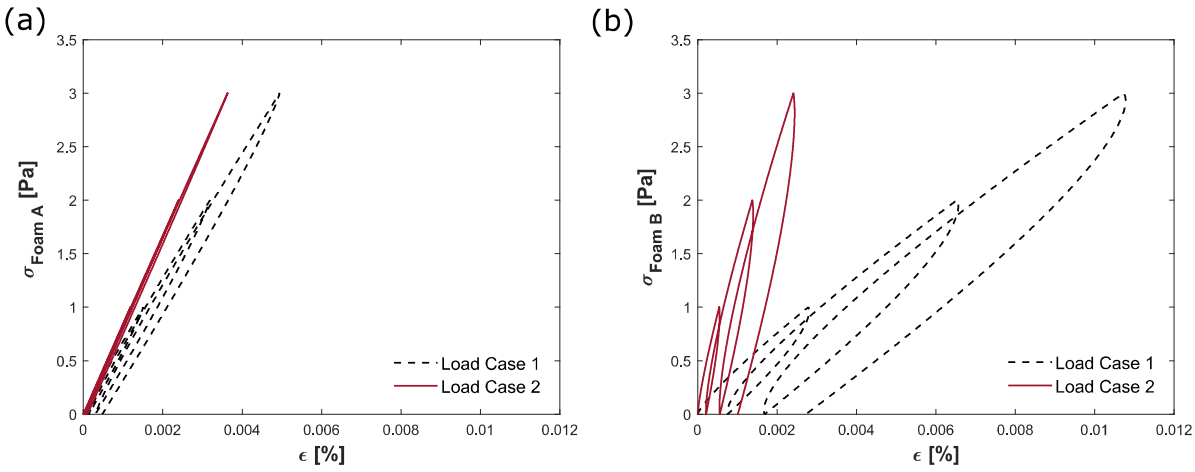

Fig. 12. Comparison between the responses of the two cyclic load cases at 20°C. (a) Foam A and (b) foam B.

A comparison between the stress-strain responses obtained for each loading-unloading scenario is shown in Fig. 13. For the first load case, foam A requires more force to achieve the same amount of strain $\varepsilon(t)[\%]$ than foam B. For the second load case, on the other hand, foam A deforms more easily. This comparison supports the idea that foam B has more energy dissipation capacity than foam A. These results are consistent with the strong viscoelastic behavior observed on the experimental master curves of foam B.

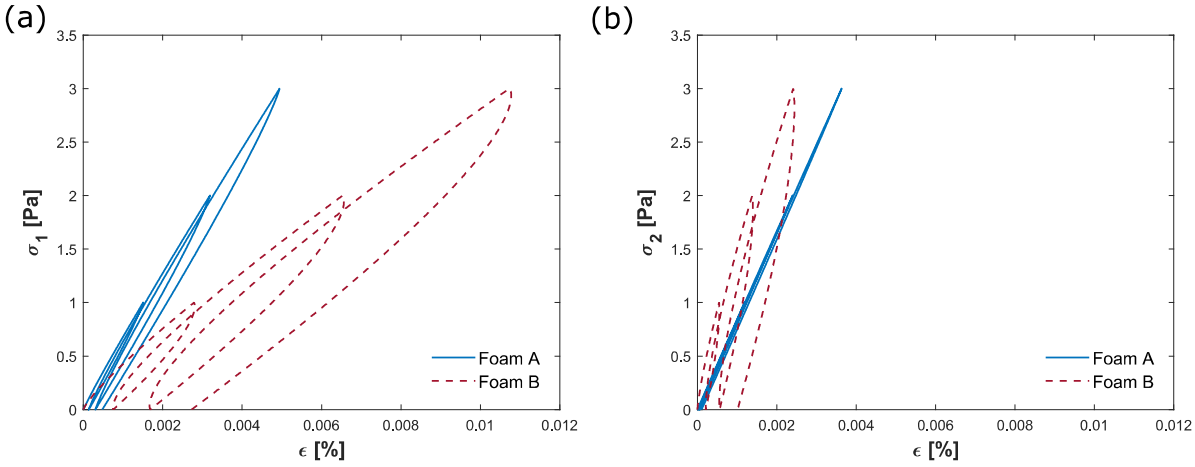

Fig. 13. Stress-strain responses obtained for each scenario at 20°C. (a) Load case 1 and (b) load case 2.

As the investigated materials presented thermo-rheological simple behavior, the influence of temperature can also be taken into account in these predictions by means of the calibrated WLF equation. The complex shear modulus and the corresponding model parameters can be assessed at any desired temperature, and so, the physical behavior of the material can be described. To evaluate this dependency, let us consider a prescribed stress history that consists of only one cycle of loading-unloading with a time scale of the order of 10^0 s. The complete loading-unloading cycle takes 2.5 s with a maximum stress level σ_{max} of 5.0 Pa, as represented in Fig. 14.

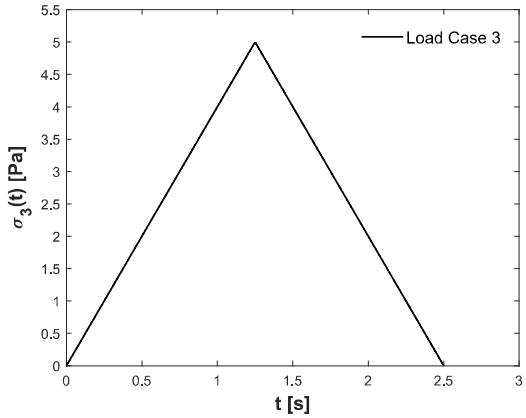

Fig. 14. Prescribed stress history (load case 3) for the study of temperature effects in hysteresis cycles.

Figure 15 compares the results at four temperatures (same as experimental tests). For both materials, the energy loss increased significantly by varying the temperature from -10°C to 20°C: the dissipation increased almost 7 times for foam A and 4 times for foam B. This feature can be related to molecular motion of polymer chains: as temperature increases, the mobility of the chains increases, which means that the material can dissipate energy better. As in load cases 1 and 2, foam B presents a better capacity to dissipate energy than foam A at all analyzed temperatures.

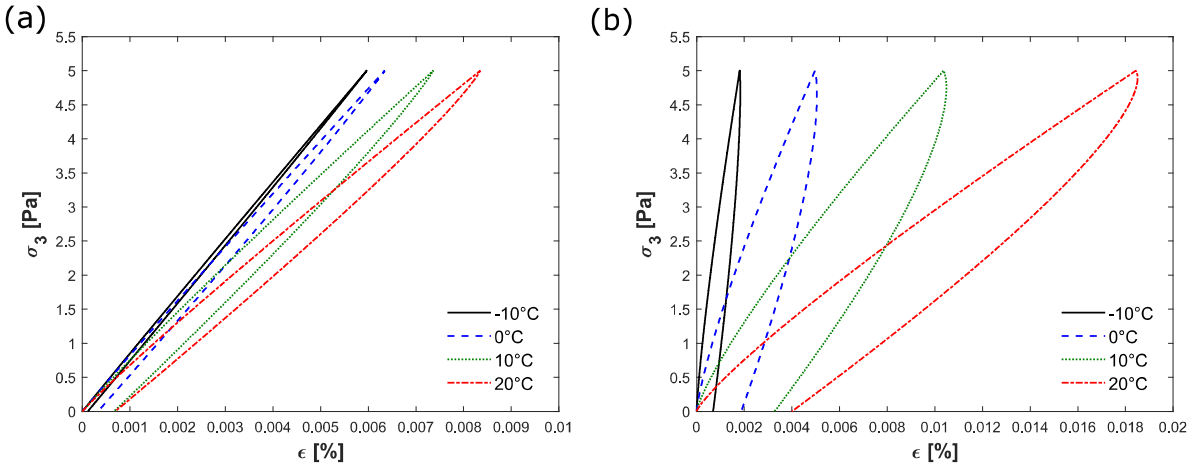

Fig. 15. Stress-strain responses for cyclic load case 3 at four different temperatures. (a) foam A and (b) foam B.

4.2. Vibrations of Simply Supported Panels

In order to explore the vibration damping behavior of the investigated polymeric foams, finite element simulations of simply supported panels in two structural configurations are performed as shown in Fig. 16. The first configuration is an aluminum panel (see properties in Table 3) of dimensions 0.420 × 0.360 × 0.003 m, whereas the second configuration is composed of the same aluminum panel with a bonded free-layer of foam (see properties in Tables 1 and 2) of dimensions 0.420 × 0.360 ×0.025 m. The goal in studying these two configurations is to investigate the effect of the porous layer on the dynamics of the panel, in particular in terms of damping.

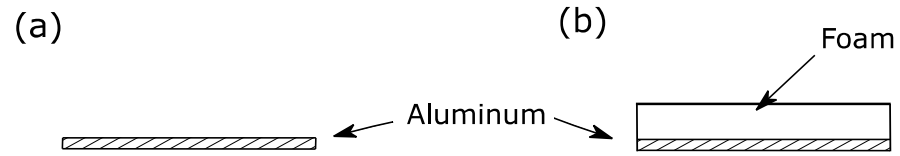

Fig. 16. Two configurations of simply supported panels for the study of vibration damping performance. (a) Bare aluminum panel and (b) aluminum panel with a bonded free layer of polymeric foam.

Table 3 Properties considered for the aluminum panel, where $\boldsymbol{E}$ is the Young's modulus, $\boldsymbol{\eta}$ is the structural damping, $\boldsymbol{\nu}$ is the Poisson's ratio and $\boldsymbol{\rho}$ is the density.

Property	E [Pa]	η	ν	ρ [kg/m^3]
	69×10^9	1×10^{-3}	0.35	2700

In both cases, the discretization of the equations of motion via the finite element method leads to

$$[\mathbb{K} - \omega^2 \mathbb{M}]\boldsymbol{U}(\omega) = \boldsymbol{F}, \tag{11}$$

where $\mathbb{K}$ and $\mathbb{M}$ are, respectively, the global stiffness and mass matrices, $\boldsymbol{U}(\omega)$ is the displacement vector at the angular frequency ω and $\boldsymbol{F}$ is the nodal load vector.

For the first configuration, the bare aluminum panel is modeled as an elastic material with a constant structural damping η. In this sense, the stiffness matrix becomes complex such as $\mathbb{K}^* = (1 + j\,\eta)\mathbb{K}_E$, where $\mathbb{K}_E$ is the elastic stiffness matrix.

For the second configuration, the aluminum panel is still modeled as an elastic material and the foam is herein modeled as a monophasic viscoelastic solid. As described in section 3.1, the foams tested in this work are assumed isotropic and with a constant Poisson's ratio. This implies that Young's modulus and shear modulus have the same frequency-dependency, as evidenced by Eq. (5). Therefore, the global stiffness matrix $\mathbb{K}$ becomes frequency-dependent such as $\mathbb{K}^*(\omega) = \mathbb{K}_E + G^*(\omega)\mathbb{K}_V^0$, where $\mathbb{K}_V^0$ is the stiffness matrix related to the viscoelastic component of the structure computed for a unit shear modulus and $G^*(\omega)$ is the complex shear modulus given by Eq. (4).

In the finite element models, a unit load is applied to excite the structures at coordinates $x = 0$ m, $y = 0.08$ m and $z = 0.08$ m. All layers are meshed with 20-node hexahedral elements, leading to 32931 (resp. 89487) degrees of freedom for configuration 1(resp. configuration 2). Geometries and meshes are generated with GMSH (Geuzaine and Remacle, 2009). Furthermore, frequency responses are computed by the direct method on the frequency range [0-800] Hz, with a frequency step of 0.5 Hz, in Matlab® software. This low-frequency range limits the influence of the fluid phase and is also associated with structural vibrations.

Figure 17 compares the frequency responses of all cases studied. One can note that adding a free layer of foam A to the aluminum panel did not lead to great changes in the frequency response, but a significant damping was introduced in the system when considering foam B. This difference becomes more evident as frequency increases and can be related to the frequency-

dependent behavior of foams. For instance, the addition of polyurethane foam reduced the resonant magnitude of the first mode by approximately 15% (around 10 dB) and that of the ninth mode by 26% (around 25dB). Therefore, it suggests that foam B can be tailored to damp structural vibrations.

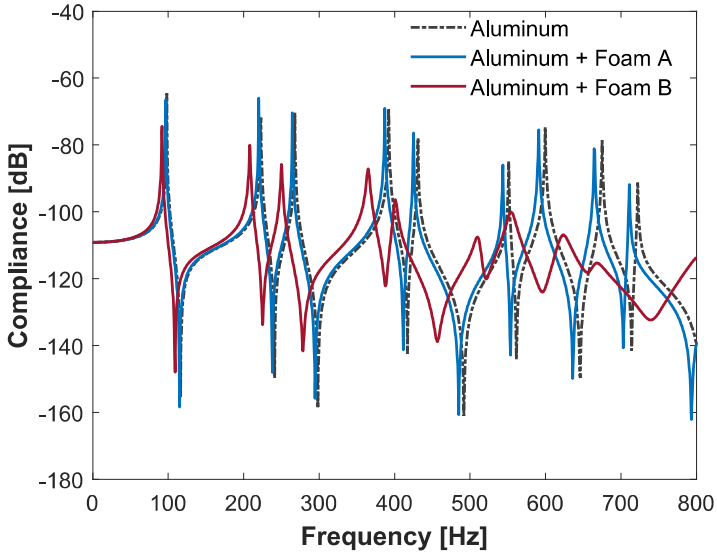

Fig. 17. Comparison between the frequency responses obtained for each configuration of the simply supported panel analyzed.

An important point that should also be investigated when studying the damping performance of a material is how much mass it adds to the whole structure. Table 4 compares the mass added in kilograms [kg] and in percentage [%]. As expected because of their densities, foam B introduces more mass to the system than foam A. However, this added mass is not so significant to the overall weight of the structure.

Table 4 Added mass of the vibration damping treatment.

Material	Foam A	Foam B
Added Mass [kg]	0.04	0.18
Added Mass [%]	3.09	14.81

5. Conclusions

This work dealt with the characterization, modeling and predictions of the mechanical behavior of two different types of polymeric foams. The investigations focused on the damping performance of these foams when considering only the viscoelasticity of their polymer skeletons.

Experimental measurements were carried out in a torsional rheometer in the very low-frequency range at various temperatures. Different time-dependent behaviors were evidenced, representative of the variety of foam types. Despite the variability which can generally be observed when measuring the elastic properties of foams (Bonfiglio *et al.*, 2018), experimental results are consistent with results from the literature. Therefore, the measured viscoelastic properties were fitted by a four-parameter fractional derivative model. Good correlation between experimental data and model predictions was observed, especially for the shear storage modulus. Additional experimental data may be required to improve the fitting accuracy of the shear loss modulus of foam A, which could not be performed due to the limitations of the characterization procedure.

Afterwards, two numerical simulations were carried out to investigate the dissipation of mechanical energy by foams. The first numerical study shows how the calibrated viscoelastic model can be implemented in the time domain to provide predictive scenarios of cyclic stress, encompassing different rates. Results evidenced hysteresis in the responses of both foams, showing the influence of the stress level and its rate on the loops. In the second numerical simulation, the calibrated models were input in finite element models to evaluate the applicability of these foams to achieve structural vibration damping. Results demonstrated that it is possible to achieve an interesting damping performance with a negligible increase in mass.

The predictions from these numerical analyses indicate that the energy dissipation capacity of foams can be estimated in the low-frequency range, even when considering only the viscoelasticity of their skeleton. It means that this numerical approach may be used in the pre-design of structures integrating foams as passive damping treatments.

These results motivate additional experiments to test the validity of the hypotheses considered in this work. Moreover, the estimation of viscoelastic properties using inverse techniques, such as in the work of Rouleau *et al.* (2016), would enable insights into the validity of the proposed approach at higher frequency.

Acknowledgements

This study was financed in part by the CAPES/COFECUB program under the grant number 88887.299103/2018-00.

Data availability

The raw/processed data required to reproduce these findings cannot be shared at this time due to technical or time limitations.

References

Bagley, R.L., Torvik, P.J., 1986. On the Fractional Calculus Model of Viscoelastic Behavior. J. Rheol. (N. Y. N. Y). 30, 133–155. https://doi.org/10.1122/1.549887

Bagley, R.L., Torvik, P.J., 1983. A Theoretical Basis for the Application of Fractional Calculus to Viscoelasticity. J. Rheol. (N. Y. N. Y). 27, 201–210. https://doi.org/10.1122/1.549724

Bonfiglio, P., Pompoli, F., Horoshenkov, K. V., Rahim, M.I.B.S.A., Jaouen, L., Rodenas, J., Bécot, F.X., Gourdon, E., Jaeger, D., Kursch, V., Tarello, M., Roozen, N.B., Glorieux, C., Ferrian, F., Leroy, P., Vangosa, F.B., Dauchez, N., Foucart, F., Lei, L., Carillo, K., Doutres, O., Sgard, F., Panneton, R., Verdiere, K., Bertolini, C., Bär, R., Groby, J.P., Geslain, A., Poulain, N., Rouleau, L., Guinault, A., Ahmadi, H., Forge, C., 2018. How reproducible are

methods to measure the dynamic viscoelastic properties of poroelastic media? J. Sound Vib. 428, 26–43. https://doi.org/10.1016/j.jsv.2018.05.006

Butaud, P., Ouisse, M., Placet, V., Renaud, F., Travaillot, T., Maynadier, A., Chevallier, G., Amiot, F., Delobelle, P., Foltête, E., Rogueda-Berriet, C., 2018. Identification of the viscoelastic properties of the tBA/PEGDMA polymer from multi-loading modes conducted over a wide frequency–temperature scale range. Polym. Test. 69, 250–258. https://doi.org/10.1016/j.polymertesting.2018.05.030

Cuenca, J., Van Der Kelen, C., Göransson, P., 2014. A general methodology for inverse estimation of the elastic and anelastic properties of anisotropic open-cell porous materials - With application to a melamine foam. J. Appl. Phys. 115. https://doi.org/10.1063/1.4865789

Dae Han, C., Kim, J.K., 1993. On the use of time-temperature superposition in multicomponent/multiphase polymer systems. Polymer (Guildf). 34, 2533–2539. https://doi.org/10.1016/0032-3861(93)90585-X

Dauchez, N., Sahraoui, S., Atalla, N., 2003. Investigation and modelling of damping in a plate with a bonded porous layer. J. Sound Vib. 265, 437–449. https://doi.org/10.1016/S0022-460X(02)01454-2

Dealy, J., Plazek, D., 2009. Time-Temperature Superposition - A Users Guide. Rheol. Bull. 16–31.

Dovstam, K., 2000. Augmented Hooke's law based on alternative stress relaxation models. Comput. Mech. 26, 90–103. https://doi.org/10.1007/s004660000157

Ehrig, T., Modler, N., Kostka, P., 2018. Compression and frequency dependence of the viscoelastic shear properties of flexible open-cell foams. Polym. Test. 70, 151–161. https://doi.org/10.1016/j.polymertesting.2018.06.036

Enelung, M., Olsson, P., 1999. Damping described by fading memory - analysis and application to fractional derivative models. Int. J. Solids Struct. 36, 939–970. https://doi.org/10.1016/S0020-7683(97)00339-9

Etchessahar, M., Sahraoui, S., Benyahia, L., Tassin, J.F., 2005. Frequency dependence of elastic properties of acoustic foams. J. Acoust. Soc. Am. 117, 1114–1121. https://doi.org/10.1121/1.1857527

Ferry, J.D., 1980. Viscoelastic Properties of Polymers, Third. ed, New York: Wiley.

Fowler, B., Rogers, L., 2006. A New Approach to the Vertical Shift of Complex Modulus Data for Damping Polymers Wicket Unedited Unshifted. Proc. 77th Shock Vib. Symp. 22.

Gama, N. V., Ferreira, A., Barros-Timmons, A., 2018. Polyurethane foams: Past, present, and future. Materials (Basel). 11. https://doi.org/10.3390/ma11101841

Geslain, A., Dazel, O., Groby, J.-P., Sahraoui, S., Lauriks, W., 2011. Influence of static compression on mechanical parameters of acoustic foams. J. Acoust. Soc. Am. 130, 818–825. https://doi.org/10.1121/1.3605535

Geuzaine, C., Remacle, J., 2009. Gmsh: A 3-D finite element mesh generator with built-in pre- and post-processing facilities. Int. J. Numer. Methods Eng. 79, 1309–1331. https://doi.org/10.1002/nme.2579

Gurp, M. van, Palmen, J., 1998. Time-temperature superposition for polymeric blends. Rheol. Bull. 67 (1), 5–8.

Jaouen, L., Renault, A., Deverge, M., 2008. Elastic and damping characterizations of acoustical porous materials: Available experimental methods and applications to a melamine foam. Appl. Acoust. 69, 1129–1140. https://doi.org/10.1016/j.apacoust.2007.11.008

Khemani, K.C., 1997. Polymeric Foams: An Overview, in: Polymeric Foams, ACS Symposium Series. American Chemical Society, p. 1. https://doi.org/doi:10.1021/bk-1997-0669.ch001

Lakes, R.S., 2009. Viscoelastic materials. Cambridge University Press, Cambridge ; New York.

Makris, N., 1997. Three-dimensional constitutive viscoelastic laws with fractional order time derivatives. J. Rheol. (N. Y. N. Y). 41, 1007–1020. https://doi.org/10.1122/1.550823

Mariez, E., Sahraoui, S., Allard, J.F., 1996. Elastic Constants of Polyurethane Foam's Skeleton for Biot Model, in: Noise Control Engineering: Internoise 96. Liverpool, pp. 951–954.

Placet, V., Foltête, E., 2010. Is Dynamic Mechanical Analysis (DMA) a non-resonance technique? EPJ Web Conf. 6, 41004. https://doi.org/10.1051/epjconf/20100641004

Podlubny, I., 2000. Matrix approach to discrete fractional calculus. Fract. Calc. Appl. Anal. 3, 359–386.

Pritz, T., 1996. Analysis of four-parameter fractional derivative model of real solid materials. J. Sound Vib. 195, 103–115. https://doi.org/10.1006/jsvi.1996.0406

Rodríguez-Pérez, M.A., Almanza, O., Del Valle, J.L., González, A., De Saja, J.A., 2001. Improvement of the measurement process used for the dynamic mechanical characterization of polyolefin foams in compression. Polym. Test. 20, 253–267. https://doi.org/10.1016/S0142-9418(00)00030-1

Rouleau, L., Deü, J.-F., Legay, A., 2016. Inverse characterisation of frequency-dependent properties of adhesives. J. Phys. 744, 1–7. https://doi.org/10.1088/1742-6596/744/1/012193

Rouleau, L., Deü, J.-F., Legay, A., Le Lay, F., 2013. Application of Kramers-Kronig relations to time-temperature superposition for viscoelastic materials. Mech. Mater. 65, 66–75. https://doi.org/10.1016/j.mechmat.2013.06.001

Rouleau, L., Pirk, R., Pluymers, B., Desmet, W., 2015. Characterization and Modeling of the Viscoelastic Behavior of a Self-Adhesive Rubber Using Dynamic Mechanical Analysis Tests. J. Aerosp. Technol. Manag. 7, 200–208. https://doi.org/10.5028/jatm.v7i2.474

Sahraoui, S., Guo, X., Yan, G., Parmentier, D., 2015. Mechanical characterisation of acoustic foams: Fractional derivatives approach, in: Euronoise 2015. pp. 1185–1189.

Sahraoui, S., Zekri, N., 2019. On fractional modeling of viscoelastic foams. Mech. Res.

Commun. 96, 62–66. https://doi.org/10.1016/j.mechrescom.2019.03.004

Schwarzl, F., Staverman, A.J., 1952. Time-Temperature Dependence of Linear Viscoelastic Behavior. J. Appl. Phys. 23, 838. https://doi.org/10.1063/1.1702316

Sfaoui, A., 1995. On the viscoelasticity of the polyurethane foam. J. Acoust. Soc. Am. 97, 1046–1052. https://doi.org/10.1121/1.412987

Srivastava, V., Srivastava, R., 2014. On the polymeric foams: Modeling and properties. J. Mater. Sci. 49, 2681–2692. https://doi.org/10.1007/s10853-013-7974-5

Williams, M.L., Landel, R.F., Ferry, J.D., 1955. The Temperature Dependence of Relaxation Mechanisms in Amorphous Polymers and Other Glass-forming Liquids. J. Am. Chem. Soc. 77, 3701–3707. https://doi.org/10.1021/ja01619a008